

PHOTON PARTICLE MODEL DISPERSION EXPERIMENT

VIDERE MACULA

VIDERE MACULA CURRUNT

John E. Blaszyński

Abstract— A photonics experiment is considered to validate a standalone particle model for the photon predicted by a new dynamic space metric where spin creates a compression of physical space to create a particle Ether which defines physical space and creates all other particle anti-particle pairs. (See VII Appendix) The experiment is performed under single and double slit boundary conditions where slits are modeled as waveguides to evaluate the dispersive photon force predicted by Equation 2.

The model uses the particles dispersive force which predicts the wave theory signature plus single and double slit intensities as a function of slit width d .

The number of bouncing photons relative to the ideal distribution or bulk loading factor was measured as

$$f_b \left(\frac{t}{d} \right) = \frac{3\pi}{40} \log_2 \left(64 \frac{t}{d} \right) + 0.4904; R^2 = 0.9599$$

The single slit and double slit Intensities are predicted as $I_s \propto \left(\frac{\pi d}{\lambda} \right)^2$; $I_D \propto \left(\frac{\pi d}{\lambda} \right)^4$ and were measured as $\left(\frac{\pi d}{\lambda} \right)^2$; $\left(\frac{\pi d}{\lambda} \right)^{3.7}$ respectively at close to ideal. (Particle bounce loading factor $f \left(k_0, \frac{t}{d} \right) = 1$ and/or double slit spacing $m = 1$)

An Error Plot for single slit is analyzed after data are normalized to 100% of the predicted intensity of wave theory with measured values varying from 48% to 172% for the single slit. As a result of slit geometry $f \left(k_0, \frac{t}{d} \right)$ predicts these anomalies. A periodic element was noted for k_0 with a best case $R^2 = 0.486$ which decreased with k_0 amplitude. The error was a mean amplitude shift with slope s ($error = sx + b$) which was found to be a function of $\frac{t}{d}$, where t is slit thickness.

The double slit distribution is a Bayesian probability given single slit distribution. The varied effect of Multi zone dispersion predicted to vary with slit spacing m was detected. The particle migration factor $Kmf_n = f \left(\frac{M_{n-1}}{M_n} \right)$ a measure of relative intensity due to photon density, reliably predicted error slope and distribution errors and the absence of wave theory harmonics in far field. Where wave theory had substantial errors the particle distribution model yielded better results, while a function of Kmf_n compensated for the distribution error.

Sufficient data did not exist to quantify a general equation for $f \left(k_0, \frac{t}{d} \right)$ or $f \left(\frac{M_{n-1}}{M_n} \right)$ however the results indicate that a standalone particle distribution model has merit and should be further investigated.

Index Terms—Dark energy; Elementary particle vacuum; Elementary particles; Nanophotonics; Photonics; Particle beam optics; Physical theory of diffraction; Quantum vacuum; Resonance light scattering

Introduction*A. Evidence of Particle Distribution and Bounce*

The single slit *sincx* signature can be demonstrated to exist in edge diffraction where the particles could likely have bounced off the edge, while the signature from the light that bends behind the obstruction “decreases rapidly and is negligible within a few wavelengths of the edge.”ⁱ A visual inspection of typical results for a near field student photonics experiment at Munster University in Germany (<https://en.fh-muenster.de/photonik/TO4.php>) or Dr. Richard Haskell’s single slit Fresnel diffraction experiment slides indicate that particles in near field appear to be migrating across the slit as the two main maximums migrate towards the center of the slitⁱⁱ while analyzing the single obstruction signature, laser based small angle scatter models are most common and can detect particles in size from nm to mmⁱⁱⁱ while the Physical Theory of Diffraction makes better predictions for large bodies and was used to develop stealth technology.^{iv}

As a precursor to the distribution model experiment, Niagara College photonics students were asked to place a secondary single slit in the primary single slit signature. Wave theory predicts that placing the secondary single slit at the primary single slit minimums (assumed to be destructive interference due to its 180 degree phase shift) should generate a phase shifted single slit signature.¹ Although students could recreate a signature by using the secondary maximums no signature or energy above ambient was evidenced at the minimums.^v Alternatively microwave engineers consider propagation modes such that “the mode can be thought of as two plane waves bouncing off of the top and bottom plates.”^{vi} Although in a waveguide the plane waves alternatively bounce between the plates or waveguide walls multiple times, it was this impetus that inspired the waveguide model with a single bounce for the slit.

A quantum analysis of this particle bounce in the absence of the main particle beam was performed by introducing photons via a fiber optic cable to a circular waveguide cavity close to the concave edge.^{vii}

Manuscript received February 19, 2015

John E. Blaszyński was with the Electrical Engineering and Engineering Math Departments, Mohawk College, Hamilton, Ontario.

B. Theoretical Particle Creation

A new Dynamic Space Metric (see VII Appendix), DSM is proposed similar to Minkowski space, however space and time are parallel and confluent. From the simple equation $d = Ct$ where d is distance, C is speed of light and t is time, the Norm in static Euclidean Space becomes:

$$\|s\| = \|Ct\| = \sqrt{x^2 + y^2 + z^2} = Ct \quad (1)$$

In DSM, circular motion at the speed of light creates an almost infinite (quasi-infinite) compression of physical space. This creates a variable density piece of string made of compressed physical space that can be modeled as a particle. The process is analogous to creating a raindrop by condensing the moisture in the atmosphere. This particulate is assumed to be a Radiating Antiparticle (RAP). Based on the assumption that 2 of these particulate make up the particle antiparticle pair of the photon, a particle model is proposed. This zero energy photon (Ether) defines space and time in this metric.

Relying on $d = Ct$ to define the fixed distance and create stability between the two particulate both particulate will continue to spin at the speed of light and have no relative change in d if they are out of phase by 60° .

Assuming Planck's constant equals $h = m_e \frac{\sqrt{3}}{2} C \frac{\sqrt{3}}{2} R_{RAP}$ where the radius of the particulate $R_{RAP} = 5.14879015 \times 10^{-13} \text{m}$, this particle-antiparticle has a quiescent energy $E_q = \frac{3}{8} m_e C^2$ and a frequency of $f_{RAP} = \frac{5.822580631}{2\pi} \times 10^{20}$. This frequency may be the carrier frequency of our universe while the quiescent energy may be what Hasenohrl discovered when he measured blackbody radiation relative to the Ether as $E = \frac{3}{8} m_e C^2$ in 1904 one year prior to Einstein's SRT that yielded $E = m_e C^2$.^{viii} The Planck-Einstein equation is consistent in this model with $\Delta E = m_e \frac{\sqrt{3}}{2} C \Delta v$ for small Δv or $\Delta E = m_e (\frac{\sqrt{3}}{2} C + \frac{\Delta v}{2}) \Delta v$. In this particle model, the ideal conditions exist for the particle-antiparticle separation at $\Delta v = \frac{\sqrt{3}}{2} C$. Therefore, $\Delta E = \frac{9}{8} m_e C^2$ and after accounting for $\frac{1}{8} m_e C^2$ bonding energy the remaining detectable particle energy is $E = m_e C^2$ relative to the particle quiescent energy and hence the creation of what we perceive as matter.

It should be noted that in this metric space the particle only exists in one dimension and as a quasi-two-dimensional particle does not respond to conventional gravity in free space since gravity exists relative to the Ether and is a multidimensional effect that increases with the number of dimensions as dimensionality decreases the propagation radius. (See VII Appendix D. *Spin Induced Fields In Dynamic Space*, E. *Rotation Induced Fields in Dynamic Space*)

The predicted force between adjacent photons is:

$$F_D \propto \frac{(2 \sin \frac{\varphi}{2})^2}{r^2} n, \quad (2)$$

where n is the number of photons, φ is the phase difference and r is the radial distance. It has two components, one in the direction of propagation and another perpendicular or dispersive or exists at an angle α or $\sin \alpha = \frac{\sqrt{3} R_{RAP}}{2 \lambda}$ (See fig A4).

The first and most obvious prediction of the particle model is the laser, since "like photons" or photons in phase do not experience a dispersive force as well as Snell's law which results from a net force of zero between photons in respective mediums.

A distribution model based on the cumulative force between photons was developed. A denser particle beam would be analogous to pushing a boat away from a dock while as far field is approached the interaction becomes similar to pushing one boat off another. The later becomes more noteworthy in the double slit set up.

An improved model of the photon would increase the resolution of signature analysis for homeland security; drug analysis etc. as did the Physical Theory of Diffraction for large scale particles composites. It would improve detection reliability while diminishing the efficacy of counter measures. Improved particle modeling of the photon could reduce collateral cell damage from radiation therapy. Mathematical model validation could prove helpful in linking String Theory and Particle Theory and improving both models.

If this dark photon is ironically dark energy and perhaps dark matter, it would address numerous discrepancies in cosmology and the quantum vacuum while a particle Ether would explain particle entanglement and the constancy of C , among other things. "Aether is currently under consideration to explain many unresolved issues in cosmology. Andreas Albrecht, a cosmologist at the University of California, Davis, believes that this ether model is worth investigating further. "We've hit some really profound problems with cosmology, with dark matter and dark energy," he says. "That tells us we have to rethink fundamental physics and try something new."^{ix}

With respect to the quantum vacuum where many including Paul Dirac have commented that it may in fact be a Particulate Aether, Robert B. Laughlin, Nobel Laureate in Physics states "The modern concept of the vacuum of space, confirmed every day by experiment, is a relativistic ether. But we do not call it this because it is taboo."^x

A first order model of the EM and gravitational forces of the electron created in DSM reliably predicts the Coulomb Force gravitational constant G (error of 0.25% 1.7% respectively) based on the propagation radius (Bohr radius). Assuming bonding of three particle anti particle pairs makes a neutron and two particle anti particle pairs to make a proton (one antiparticle becomes a quark), predicts a G with an error of about 6%, the ability of the proton to accept an electron and the Neutron decay to the more stable Proton, electron and high energy antiparticle or anti electron neutrino as well as the mass discrepancy of approximately $2.5 m_e$.

Although everything in this model is a result of "warping space with time" the mass of one electron, m_e is used to explain the concept in terms of simple Newtonian mechanics. A particle understanding in this model of Planck's constant $h = m_e \frac{\sqrt{3}}{2} C \frac{\sqrt{3}}{2} R_{RAP}$, should be a powerful Quantum Mechanical tool.

The infamous single and double slit experiments are used to quantify the standalone particle model predictions to verify the efficacy of the foundational model. Particle bounce is assumed to initiate the process that creates the intensity signature and evidence of this bounce

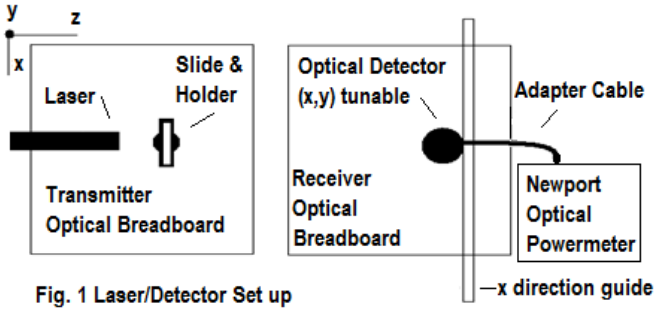


Fig. 1 Laser/Detector Set up

in conjunction with the predicted photon to photon force (which likely creates strong force) is required to validate the model.

II. EXPERIMENT

A. Apparatus

Carleton University/Algonquin College Photonics and Fiber Optics Laboratory 1385 Woodroffe Avenue
Ottawa, Ontario K2G 1V8 June 23 to June 25, 2014

Red Laser(1) Rated Output <5mW,632.8nm (measured output 1.3mW)

Red Laser(2) Rated Output <10mW,633nm (measured output 6.8mW)

Newport Optical Power Meter Model 1830-C w/Newport Universal Fiber Optic detector model 818-1S-1 (S/N 1195) (M@1)

Photo Meter-Industrial Fiber Optics (M@2)

#Single/Double Slits Slides-- Advanced Optics (S@1,s@3)

##(Courtesy Frank Benko, Brock University Physics Lab)

##Leybold Double Slit Slide (S@2)

##Microscope and AmScope MT300 CCD camera.

(Courtesy Guillermo Bernal, Carleton Univ. Physics Lab)

B. Experimental Focus

The experiment was conducted to determine if particle bounce patterns could be identified relative to slit geometry. The detection of polarity changes was ruled out since although a clean bounce is predicted off the slit wall, polarity modulation may occur as bouncing photons cross the laser beam which was modeled as a particle beam. Alternatively signature analysis by analysing intensity was chosen as this could be used to identify evidence of the predicted photon to photon force. The focus was on identifying predictable patterns and not quantifying them.

Data was collected at the peak of each secondary maximum, I_n and analyzed relative to wave theory predictions for anomalies.

C. Set Up

The use of equipment and setup recommendations were generously provided by Dr. Abdul Al-Azzawi Algonquin College/Carleton University Photonics and Information Technology Professor. Given obvious space and laser power limitations, consideration was given to signature intensity versus distance between maxima for the double slit set ups.

D. Procedure

The laser was focused on the opposite lab wall and then for each slit configuration the signature was tuned by setting the slide holder to an angle 0° (perpendicular to z) and the x, y position was adjusted to level and visually maximize the intensity. The distance between maxima was adjusted by changing z , with $z \sim 10ft$ for the single slit experiments using slide S@1 and double slits with slide S@2 and $z \sim 30ft$ for the double slit experiments using slide S@3. The minimum distance between maxima was about $3/8''$ for modulation factor $m=12.5$ ($d = 0.04mm$ and slit spacing $0.5mm$) while the single slit measurements had a minimum $1''$ between maxima. For the M@1 configuration, the Optic Detector aperture was $0.125''$ and the power meter remained on for the entire experiment. This gave measurements in excess of 99% of peak while ambient noise was reduced to and measured periodically at $0.16 nW$ for S@3 and $0.12nW$ for S@1 and S@2. A maximum of 3 significant digits were used for measurements. Assessing the actual slide measurements involved an optical microscope and CCD camera with calibrated micro ruler ($0.01mm$ resolution) and as possible; extrapolating of data to determine the center location of minimums and visual observations of numerous minimums at $z \sim 45 feet$. Slide specification $m = 3.125 \pm 6.25\%$ and $m = 6.25 \pm 6.25\%$ used all three methods to ascertain $m = 3.20 \pm 0.05$ and $m = 6.40 \pm 0.05$. The other slides where measured less reliably. Slide $m = 12.5$ was determined to be $m = 12.7 \pm 0.2$ while an iterative mathematical analysis using the new model determined it to be $m = 12.7 \pm 0.1$.

E. Procedural Limitations

Given the constraints of experimental focus, time and funding, more extensive and control measurements including automatic ambient noise zeroing were precluded.

III. THEORY

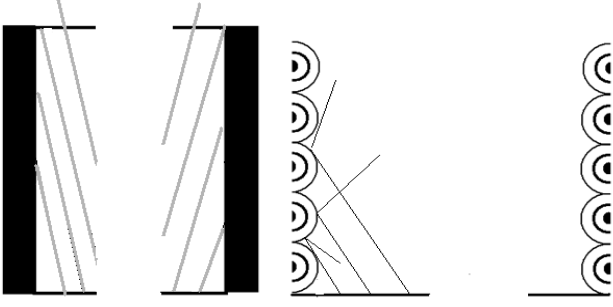
The laser is modeled as a particle beam. The beam density is simplified into 3 zones based on density (see fig. 2). Momentum of the beam is conserved in zone 1 due to particle density relative to bouncing photons. Photons bouncing off the slit wall will experience forces as they cross the beam.

A. Single slit

Using equation (2) and the assumption that the particle distribution is proportionate to the force as a function of θ , and given $\frac{2\pi d}{\lambda} \sin \theta = \varphi_1$, a first order distribution n_1 for a given d, r and λ

$$n_1(\varphi) \propto F_\theta(r^2) \propto \left(\frac{\pi d}{\lambda}\right)^2 \frac{\left(\frac{\sin \frac{\varphi_1}{2}}{\frac{\varphi_1}{2}}\right)^2}{\left(\frac{\varphi_1}{2}\right)^2} \sqrt{1 - \left(\frac{\varphi_1 \lambda}{2\pi d}\right)^2} \text{ for } \left|\frac{\varphi \lambda}{2\pi d}\right| \leq 1 \quad (3)$$

which predicts $I_0 \propto \left(\frac{\pi d}{\lambda}\right)^2$



In the previous diagram we can see how a small amount of laser dispersion will cause the photons to bounce off of the slit walls. The thicker the slit walls the more bouncing photons anticipated. In this experiment the bounce factor was assumed to be constant for all slides given the slit walls were the same thickness and the boundary where bouncing photons originate would be the same, therefore we would need to compare the amount of bouncing photons relative to non bouncing given a wider slit would have more non bouncing photons. We then note an increase in bouncing to non bouncing photons as slit width decreases. If the waveguide wall is modeled as an array of electrons and given the model predicts that the photons would be repulsed by the electrons, the reflective surface becomes bumpy at a nanolevel and the bounce factor should then become periodic.

A Particle bounce loading factor $f(k_0, t, d)$ is assumed such that k_0 reflects surface characteristics and is predicted to have a periodic component since the slit walls are Electroformed Nickel which is a face centered cubic lattice structure with a lattice parameter of 0.352 nm. Outliers are predicted since missing Nickel atoms could generate erratic bounce patterns. The thickness t for S@1, S@3 is fixed at about 8λ . As d increases it is assumed the number of forward propagating photons increases relative to the number of bouncing photons and intensity of the Secondary Maximums I_n should decrease relative to Primary Maximum I_0 . The particle distribution for the single slit follows:

$$n_1(\varphi) \propto F_\theta(r^2) \propto f(k_0, t, d) \cdot \left(\frac{\pi d}{\lambda}\right)^2 \frac{\left(\frac{\sin \frac{\varphi_1}{2}\right)^2}{\left(\frac{\varphi_1}{2}\right)^2} \sqrt{1 - \left(\frac{\varphi_1 \lambda}{2\pi d}\right)^2} \quad (4)$$

B. Double Slit

The particle distribution for one side of each single slit can be thought of as:

$$\int_0^{0+\pi} A_0 dx + \sum_{n=0}^{\infty} f(k_0, t, d) \int_{n\pi}^{(n+1)\pi} \left(\frac{\sin x}{x}\right)^2 dx \quad (5)$$

When modeled as a Bayesian probability the single slit distribution exists and then the double slit distribution exists. A higher order model for the double slit will differ significantly however a zone approximation will demonstrate that the affect of equation (2) varies with beam density.

Z1 creates the single slit distribution. Z1 will dominate the signature for small modulation factors or slit spacing m and will decrease with the succession of I_n . The density of Z1 still creates an angle θ but the effect now is also

dispersive and is approximated as $A_1 \left(\frac{\pi d}{\lambda}\right)^2 \frac{\left(\frac{\sin \frac{m\varphi_1}{2} + \frac{\pi}{2}\right)^2}{\left(\frac{\varphi_1}{2m}\right)^2}$. The

secondary Z1 effect in the double slit can also be modeled with a time shift of $\frac{\pi}{2}$ from the single slit Z1 given a Bayesian distribution.

As m increases the effect $A_2 \left(\sin \frac{m\varphi_1}{2} + \frac{\pi}{2}\right)^2$ or Zone 2 begins to dominate. This is the dispersive photon to photon force which manifests itself as particles migrate away from the signature center at I_0 .

Zone 3 is a far field effect and particle distribution is predominantly the same as that created by the initial single slit distribution. It is a product of the dispersive force between out of phase photons and generally has no further effect on distribution other than then that predicted by the particle migration factor.

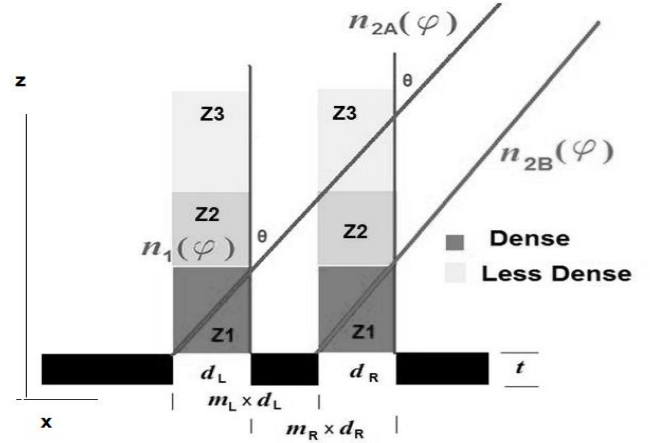


Figure 2 Distribution Zones

The general first order model distribution can be generalized as the conditional probability arising from the

following equation: $n_f(\varphi_1) = f(k_0, t, d) \left(\frac{\pi d}{\lambda}\right)^2 \frac{\left(\frac{\sin \frac{\varphi_1}{2}\right)^2}{\left(\frac{\varphi_1}{2}\right)^2}$.

$$\left(A_1 \left(\frac{\pi d}{\lambda}\right)^2 \frac{\left(\frac{\sin \frac{m\varphi_1}{2} + \frac{\pi}{2}\right)^2}{\left(\frac{\varphi_1}{2m}\right)^2} + A_2 \left(\sin \frac{m\varphi_1}{2} + \frac{\pi}{2}\right)^2\right) \quad (6)$$

Where A_1 and A_2 are likely functions of both m and n number of secondary maximums n in I_n .

IV. APPLICATION OF THEORY

1) Single slit

The Wave theory predictions and the measured results are normalized to 1 for I_0 , where wave theory

predicts the intensity: $I_0 \frac{\left(\frac{\sin \frac{\varphi_1}{2}\right)^2}{\left(\frac{\varphi_1}{2}\right)^2}$.

The normalized peak values for I_n are calculated and measured at the physical center.

In a waveguide the propagation factor is $\frac{u}{c} = \sqrt{1 - \left(\frac{\lambda}{d}\right)^2}$ and for $\left(\frac{\lambda}{d} \sim \frac{1}{32}, \frac{1}{64}, \frac{1}{128}, \frac{1}{256}\right)$ the change in $\frac{u}{c}$ is measured in parts per million. However if particle bounce is assumed this could provide a change in the period of the predicted bounce given the atomic structure of the slit wall or waveguide wall. Given these factors, detection is not thought to be realizable in this setup. Also the cosine effect

$\sqrt{1 - \left(\frac{\varphi_1 \lambda}{2\pi d}\right)^2}$ is not likely detectable due to the number of secondary maximums required to detect it and the strength and coherence of the laser required. Given the limitations of the slides available, $f(k_0, t, d)$ was modeled as $f\left(k_0, \frac{t}{d}\right)$.

2) Double slit

For the Double slit the value predicted by wave theory at center of the maximum is calculated using

$$I_0 \frac{\left(\frac{\sin \frac{\varphi_1}{2}\right)^2}{\left(\frac{\varphi_1}{2}\right)^2} \cos^2\left(\frac{m\varphi_1}{2}\right)$$

The initial distribution can be determined by computing the relative number of photons that exist for each interval or I_n .

$$\sum_{n=0}^{\infty} f\left(k_0, \frac{t}{d}\right) \left(\frac{\pi d}{\lambda}\right)^2 \int_{\frac{n\pi}{m}}^{\frac{(n+1)\pi}{m}} \left(\frac{\sin x}{x}\right)^2 dx \quad (7)$$

At this point it can be determined which zone to use to predict the double slit signature. For larger m 's it can be assumed that the distribution is mostly from zone 3 and simple particle dispersion can be used.

For smaller m 's it is assumed that zone 2 is predominant and dispersive

$$\sum_{n=0}^{\infty} f\left(k_0, \frac{t}{d}\right) \left(\frac{\pi d}{\lambda}\right)^2 \int_{\frac{n\pi}{m}}^{\frac{(n+1)\pi}{m}} \left(\frac{\sin x}{x}\right)^2 \left(\sin x + \frac{\pi}{2}\right)^2 dx \quad (8)$$

For very small m 's ($m < 2$) the zone 1 will dominate but it is predicted to have both a directional component and a dispersive component.

$$\sum_{n=0}^{\infty} f\left(k_0, \frac{t}{d}\right) \left(\frac{\pi d}{\lambda}\right)^2 \left(\frac{\pi d m^2}{\lambda}\right)^2 \int_{\frac{n\pi}{m}}^{\frac{(n+1)\pi}{m}} \left(\frac{\sin x}{x}\right)^2 \frac{(\sin mx + \frac{\pi}{2})^2}{(mx)^2} dx \quad (9)$$

The particle migration factor $Km f_n = f\left(\frac{M_{n-1}}{M_n}\right)$ is an effect approximated by the initial distribution of photons from the single slit signature. A first order model uses the ratio of photons at the previous maximum M_{n-1} to the current maximum M_n . It can be used to predict the error slope and the correction factor for particle migration into areas where wave theory predicts few should exist.

V. RESULTS AND DISCUSSION

A. Single Slit

1) Validity of $I_0 \propto \left(\frac{\pi d}{\lambda}\right)^2$ prediction

Convincing data to support the proposed particle model was found by measuring the particle density at I_0 for a fixed radial distance r from the slit aperture. The $I_0 \propto \pi d \lambda^2$ prediction was evaluated and the measured results indicate the intensity of the stable signatures increased by

n	t/d	d mm	Aperture Intensity mW**	I_0 Intensity nW @10ft	I_0 Intensity nW@?	$\frac{I_n}{I_{n-1}} = \left(\frac{d_n}{d_{n-1}}\right)^\alpha$ $\alpha @ 10ft$ $\alpha @ ?$	
1	1/4	0.02	0.2*	68	74-82	-	-
2	1/8	0.04	0.37	178	189	1.39	1.36
3	1/16	0.08	0.76	740	730	2.06	1.95
4	1/32	0.16	1.48	2900	2800	1.97	1.94

Table I * approximated (I_0 was not stable) ** Measured with M@2 (larger aperture)

about $\left(\frac{\pi d}{\lambda}\right)^{2.06}$ and $\left(\frac{\pi d}{\lambda}\right)^{1.97}$ @ $f\left(k_0, \frac{t}{d}\right) \sim 1$. The intensity between the unstable $\frac{t}{d} = 1/4$ and stable $\frac{t}{d} = 1/8$ was $\left(\frac{\pi d}{\lambda}\right)^{1.4}$ (note the $\frac{t}{d} = 1/4$ intensity at slit aperture was unstable and @ $f\left(k_0, \frac{t}{d}\right) \sim 0.0682x + 1.1134$) See 2) $f\left(k_0, \frac{t}{d}\right)$ Predictions. The slits were examined under microscope and the single slit slides fell well within the manufacturers specification of +/-0.005mm. The slit edges for 0.04mm, 0.08mm and 0.16mm were clean and sharp however 0.02mm slit edge was not as sharp, appeared serrated and was about 0.022mm wide. The edge resolution could be either due to slit geometry or possibly a measuring error given it was an optical microscope.

The intensity at the slide aperture was determined to increase linearly with slit width d , and hence wave theory predicts that I_0 should also increase linearly since a fixed aperture size measured the average of values within 99% of peak. Assuming a conservation of energy would dictate that the total wattage at slit aperture would equal the wattage of the wave theory signature (assuming dy is fixed) we calculate:

$$Watts = \int_{-\infty}^{\infty} I_0 \left(\frac{\sin \varphi}{\varphi}\right)^2 d\varphi = \pi I_0 \quad (10)$$

Therefore wave theory would predict a linear increase in I_0 with a linear increase in energy through the slit aperture. Hence the exponential increase in signature intensity measured was not predicted by the wave theory model but can be explained and compensated for with further wave model assumptions. Redefining $I_0 = \frac{Watts}{\iint dyd\varphi}$ or adding the assumption $r \propto d$ accounts for the wave theory discrepancy. This however is explicitly predicted by the particle model since increasing the radial distance r such that $r \propto d$ will force a linear increase in signature intensity. Given that the measurements can be thought of as watts per aperture area they are better understood as particle density measurements and this is why the particle model makes better predictions.

2) Validity of $f\left(k_0, \frac{t}{d}\right)$ Predictions

The particle bounce loading factor $f\left(k_0, \frac{t}{d}\right)$ predicts more particles will bounce relative to propagating particles for higher values of $\frac{t}{d}$, I_0 decreases while I_n increases and this could partially explain the reduced $I_0 \propto \left(\frac{\pi d}{\lambda}\right)^{1.39}$ for $\frac{t}{d} = 1/4$ and stable $\frac{t}{d} = 1/8$ since both signatures exhibit a mean amplitude shift up wards with a positive slope with respect to consecutive secondary maximums. Given a conservation of energy these particles must be dispersed from the primary maximum.

When linear regression was performed the data indicated the bounce loading factor could be modeled as $f\left(k_0, \frac{t}{d}\right) = mx + b + k_0$; where the slope s was a function of $\frac{t}{d}$ and k_0 seemed to be periodic however when a variety of measurements were done it k_0 was erratic and could also be attributed to a localized error. (See fig. 3). To determine if k_0 was a contributing factor to signature analysis the total intensity was evaluated "averaging" the effect of k_0 . When the total intensity of each $\frac{t}{d}$ was compared a bulk loading factor was determined to be:

$$f_b\left(\frac{t}{d}\right) = \frac{3\pi}{40} \log_2\left(64\frac{t}{d}\right) + 0.4904; R^2 = 0.9599$$

This established that a strong correlation existed between slit thickness and the number of relative bouncing photons. When the curve predicted by linear regression is used to predict the number of bouncing photons in the maximums not yet measured the correlation factor was seen to improve indicating that the poor correlation factors for individual $\frac{t}{d}$ curves was a result of the error k_0 contributed to a linear relationship and that in principal the curve predicted by linear regression was trend predicting. No regressive curve fitting was employed for k_0 as this would be misleading given the limited data.

The decrease in slope relative to $\frac{t}{d}$ and the mean amplitude shift down are consistent with the reduction in bouncing particles relative to forward propagating particles. The data was analyzed using several curve fitting models removing outliers and also by increasing the ambient noise value to 0.16nW. Linear regression in Fig.3 seemed to be the best fit.

Also the ideal $\left(\frac{\pi d}{\lambda}\right)^2$ or $\alpha = 2$, would be expected to occur at $f\left(k_0, \frac{t}{d}\right) = 1x + 1$. This was consistent with the data that seemed to indicate that a slope of 1 could be anticipated between $\frac{t}{d} = \frac{1}{16}, \alpha = 2.06$ and $\frac{t}{d} = \frac{1}{32}, \alpha = 1.97$.

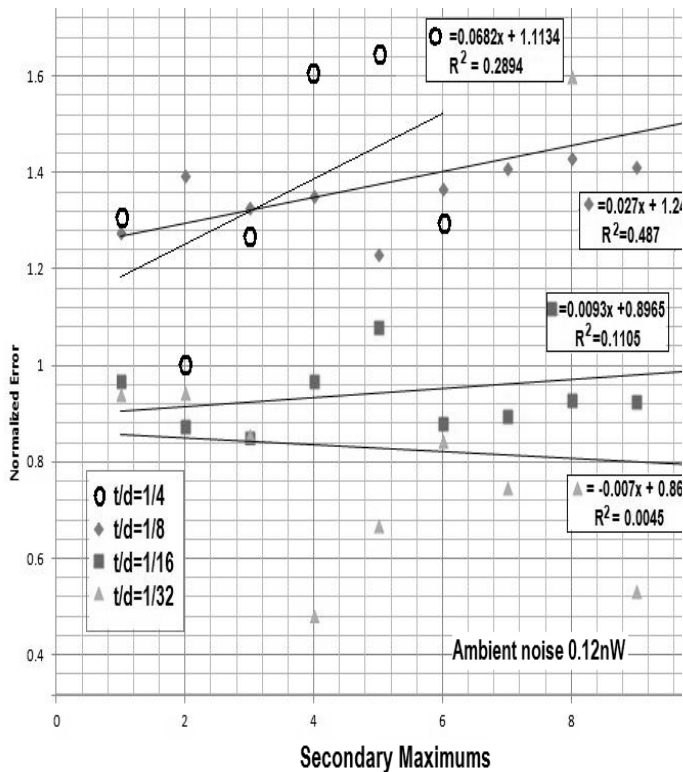


Fig. 3 Normalized Error Curve for single slit experiment

Although the data indicated the anticipated patterns of particle bounce, varying the slit thickness with respect to a fixed slit width and vice versa would provide more insight into model predictions by developing $f(k_0, t, d)$. Further due to insufficient precision and sample

size no degree of certainty could be made as to quantifiable predictions of the model and this was known from inception.

It should be noted that all data analysis relied on relative measurements so calibration and steady state errors had negligible effect. To better quantify the results more data is required. To offset the effect of slit wall surface defects several measurements should be taken at different y locations on the slit while maintaining similar throughput power ratings.

To eliminate errors due to throughput power oscillations, I_0 should be diverted by a mirror and monitored constantly and/or the throughput power should be measured immediately before and after each measurement at both the slit aperture and I_0 . Power fluctuations of I_0 can be possible even in the absence of fluctuations at the slit aperture since the particle distribution can change with negligible displacements of the slit aperture. Reducing the noise and vibrations may improve this result. It was noted that the location in the lab caused variations in the ambient noise detected so when accounting for ambient noise, calibrations should be done frequently and if possible with each measurement. $f\left(k_0, \frac{t}{d}\right) = sx + b$ is predicted to change with throughput radiated power as well as coherence. Varying the throughput radiated power by adjusting the beam intensity would demonstrate an increased offset b and/or slope s .

B. Double slit

The particle model predictions of multi zone dispersion and particle migration were observed and to a lesser degree, bounce.

1) Multi zone Dispersion

Given that some type of overlap of the three primary types of dispersion was expected a clear understanding of the double slit model was not realizable. The single slit signature was a function of Zone 1 dispersion. As expected for smaller m 's some evidence of zone 1 dispersion was evident in the double slit signatures for $m < 2.5$. As expected for smaller m 's, some evidence of zone 1 dispersion was evident in the double slit signatures for $m < 2.5$.

n	Slit Spacing m	d (measured) μm	I_0 Intensity $nW @ 10ft$	$\frac{I_n}{I_{n-1}} = \left(\frac{d_n}{d_{n-1}}\right)^{\alpha *}$
1	2.5	110	920	-
2	1.66	171	2450	2.2
3	1.25	215	5600	3.7

Table II* The double slit intensity at the slit aperture was assumed to increase linearly. Contrary to this assumption, throughput power is predicted to decrease as the slit separation factor $(m-1)$ increases. Due to particle bounce and scatter off the slit separation, more particles bounce back and the conservation of momentum will reduce the coherence of the laser entering slit aperture and consequently the density of the particle beam. This was noted as the assumption of a linear throughput for the double slit reduced $\alpha = 1.2$ for $m = 6.4 \pm 0.05$ at I_0 .

In table II it was observed that zone 1 dominance quickly fell off with m as α fell from 3.7 to 2.2. In zone 2 for

a fixed slit width the intensity fell off as m increased. For 0.08mm slits, $m=3.2\pm 0.05$ had an $I_0 = 850nW$, while $m = 6.4 \pm 0.05$ was $I_0 = 420nW$; while going from zone 2 to zone 3 for 0.04mm slits, $m = 6.4 \pm 0.05$, $I_0 = 185nW$ and $m = 12.7 \pm 0.2$, $I_0 = 125nW$. (Zone 2 approximation was the best fit for $m=3.2\pm 0.05$ while zone 3 was the best fit for $m = 12.7 \pm 0.2$.)

In fig. 4 the effect of Zone 1 dispersion likely explained the measured values above that of wave theory for the first 10 secondary maximums, while $\left(\frac{\varphi_1}{2m}\right)^2$ could explain the negative slope when regression was performed as the measured values oscillated about the first order linear approximation. Zone 3 dispersion can be noted at secondary maximums 5 and 10 as the harmonics predicted by wave theory did not exist and the particle migration factor in combination with Zone 2 dispersion was seen to create a dispersion predicted by $\sin^2\left(\frac{m\varphi_1}{2} + \frac{\pi}{2}\right)$. For smaller m 's it is expected that some of the residual effects of Zone 2 could be observable just beyond the Fresnel Zone as this zone predicts the particle distribution to have a harmonic component. As the signature extends beyond the Fraunhofer zone the signature will be periodic about $\frac{m\varphi_1}{2}$.

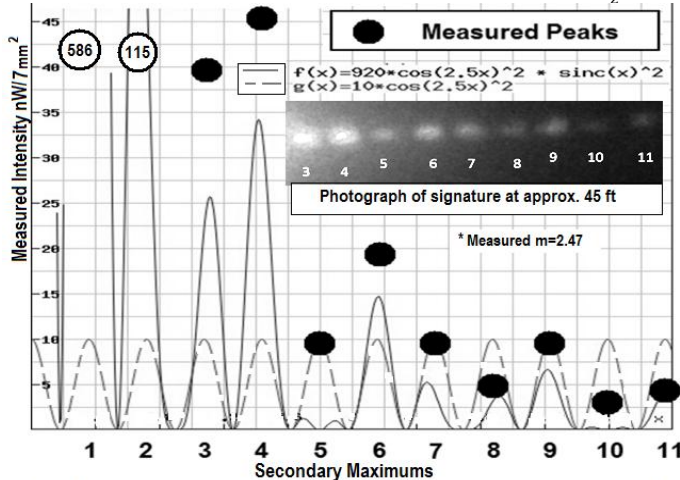


Fig. 4 Measured Maximums vs Wave Theory Predictions ($m = 2.5$)*

2. Bounce loading factor

A Lack of Symmetry using Laser 2 (<10mW) between left and right maximums was noted to be skewed on the older slides that used photographic exposure to create the slits. The microscopic measurements of $m=1.25$ +/- ? yielded $m=1.17\pm 0.1$ and $\frac{d_L}{d_R} = 100.4\% \pm 3\%$ ** or $\frac{d_L}{d_R} = 103\%$ ** . The lack of symmetry was observed on all measurements and the relative lack of symmetry ranged from 48% to 249%.

The newer slides boasted superior edge technology being comprised of electroformed nickel. The lack of symmetry was observed to be negligible, however some outliers were noted but measurements were not documented. Some lack of symmetry was noted and measured with Laser 1 (<5mW) for $m=3.2\pm 0.05$ $\frac{d_L}{d_R} = 102\% \pm 1\%$ ***. The lack of throughput power made it difficult to assess the lack of symmetry, however the distribution is probability based and the Laser 1 particle

beam would yield a smaller sample size and less reliable results. Further Zone 1 dispersion would be reduced given less particle density.

***The error discrepancy could be considered subjective and is based on the resolution of the auto exposure of CCD camera and dispersion effects through the slits created by the optical microscope. The older slide coincidentally had less symmetry between left and right slit widths d_L and d_R and although somewhat subjective less definite edges.

Some indications of bounce in the double slit signatures were identified in the lack of symmetry and although some indications of the bounce loading factor for the double slit, $f\left(k_0, \frac{t}{d}\right)$ may have existed controls for slit separation and multi zone dispersion were not implemented precluding any such conclusions.

3. Particle migration factor $Kmf_n = \frac{M_{n-1}}{M_n}$

A particle migration factor was noted as predicted by $A_2\left(\sin\frac{\varphi_2}{2} + \frac{\pi}{2}\right)^2$. This dispersion factor predicts a particle migration factor which is a function of the intensity at a specific maximum n or $Kmf_n = \frac{M_{n-1}}{M_n}$. It was a good indicator of error slope for most applications (see fig.5) where $Kmf_n = 1$ corresponded to a zero slope and $Kmf_n > 1$ indicated a positive slope while $Kmf_n < 1$ corresponded to a negative slope or $-\frac{1}{Kmf_n}$. As expected the reliability of Kmf_n increased with m . Where the single slit intensity approaches zero the measured intensity could be found by multiplying the expected value from linear regression by $\frac{Kmf}{4}@m = 3.20 \pm 0.05$ and $\frac{Kmf}{3}@m = 12.70 \pm 0.2$.

These values have no qualitative value and were found to vary depending on the variations to the distribution model used and are only probative values. Particle migration was found to predict the error in the majority of measurements and it was reasonably foreseeable in which areas it would not perform as ideal.

Particle migration factor model improvements would consider the cumulative effect of the entire particle distribution. Considering $Kmf_n = \frac{M_{n+1}}{M_n}$ would improve the model; however this effect is less dramatic since the cumulative force of the particles below M_n is significantly less than those above.

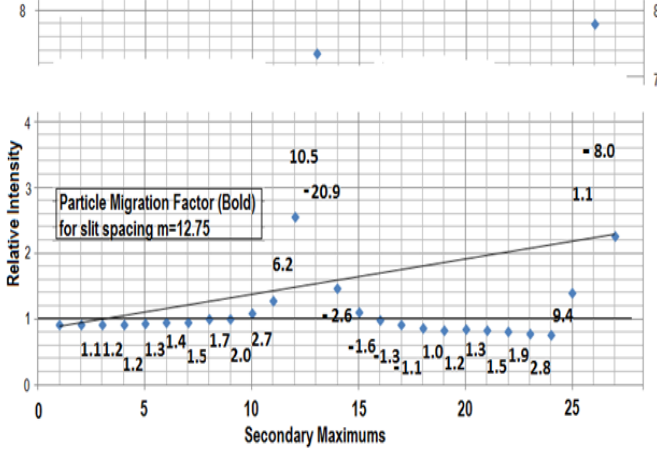


Fig. 5 Effects of Particle Migration Factor (Zone 3)

All of these factors are predicted by the fundamental equation of photon to photon force which assumes that the force is proportional to the number of photons n in Equ. 2.

VI. SUMMARY

The single slit particle model made better predictions than anticipated. This was due to its uncomplicated first order model approximations. A better understanding of the particle bounce loading factor $f(k_0, \frac{t}{d})$ could likely be realized by determining $f(k_0, t, d)$. The existence of the cosine effect or $\sqrt{1 - (\frac{\phi_1 \lambda}{2\pi d})^2}$ could be measured by using a stronger laser to reliably measure a considerable number of secondary maximums. More precise measurements and better control over slit materials could determine if the sinusoidal component from the atomic structure of the slit wall exists. Since nickel, silver and gold have a similar Face Centered Cubic structure with the lattice constants 352pm, 408 pm and 407pm a negligible change in the frequency component would be noted however the increase in electrons would likely reduce the amplitude.

Given its improved predictions for the single slit, the particle model should be further investigated for other applications.

The double slit particle model was more complicated, and a clear understanding of the predictions of each element was not possible given the overlap of the elements. Some evidence of all the predictions was evident and given controlled and exhaustive testing an understanding of each of these would improve laser signature analysis by increasing resolution and dimensionality for both homeland security and particle analysis applications and reduce the effectiveness of countermeasures.

In general the experiment was successful in demonstrating the superior predictions of the pure particle model. Although the double slit model was too complicated to make any qualitative model recommendations its predictions noted many discrepancies in the wave model that were further detected.

Known that the scope of the experiment was to validate a standalone particle model for the photon

predicted by a new dynamic metric space where a particle Ether defines physical space, the experiment can be considered a success. This new particle ether may address many shortcomings of the current models and predicts a simple creation of the universe from empty physical space and consequently merits further analysis.

VII. APPENDIX (MATH)

A. A Dynamic Metric of Space and Time

By definition $d = Vt$, where distance= velocity x time.

Let us use the axiom that $d = Ct$ in free space where C is the free-space velocity of light and develop a definition of Euclidean Space based on this observation.

This yields: $x^2 + y^2 + z^2 = s^2 = (Ct)^2$ M1

Any point on the surface or mantle of the sphere can be defined $s=f(x,y,z)=f(t)$.

In Euclidean space from $x^2 + y^2 + z^2 + (jCt)^2 = 0$ we can imply a Euclidean space exists such that (x, y, z, jCt) which is consistent with Equ. M1.

Note that in Euclidean space (x,y,z) are orthogonal and using j to represent a 90 degree phase shift implies t is parallel to s . (j is also orthogonal to the i in Euler in both space and time) To prove:

Let $\hat{x} \rightarrow$ propagation; Let $\hat{y} \rightarrow$ radius; At $t = 0, (x, y) = (0, 1)$

$$i^2 \hat{x} = -\hat{x}; i^2 \hat{y} = -\hat{y}$$

$$\therefore i\hat{x} \perp i\hat{y} \text{ or } \hat{i} \perp \hat{j}$$

Hence a two dimensional spin, \hat{i} spin and \hat{j} spin

Yields the identity: M2 $e^{i\omega t \hat{j}} \cdot e^{i\omega t \hat{i}} = e^{i\omega t \hat{i}} - \mathbf{1} + e^{i\omega t \hat{j}}$

The significance of this equation, spin and the ability to define space becomes obvious when we assume a point P in Euclidean space to be a compression of infinite degrees of orthogonal zeros. For our purposes we use an infinite series of increasing degrees of zero in a scalar context. Let $\partial n = 0$; $\partial n \partial n \ll \partial n$. Where $(\partial x, \partial y) \rightarrow (0, 0)$ and $x \times y \rightarrow 2D$; $\partial x \times y$ or $\partial y \times x \rightarrow 1D$ and $\partial x \times \partial y \rightarrow 0D$ but $n_k = \int_0^{n_k} \partial n_{k+1}$

Modeling integration as a stretch to the next orthogonal dimension we arrive at a definition of a zero dimensional point in Euclidean space:

M3

$$\int \partial x_t = \int \partial x_k + \iint_0^{x_k} \partial x_k \partial x_{k+1} + \iiint_0^{x_k, x_{k+1}} \partial x_k \partial x_{k+1} \partial x_{k+2} + \dots$$

$$x_t = x_k + \frac{x_k^2}{2!} + \frac{x_k^3}{3!} + \dots$$

A function is a stretch of a point $(\partial x, \partial y)$ and can be thought of as an array of points and point (x, y) OR (x_k, x_{k+1}) can be defined using a definite integral with the boundaries defined in x_k .

The extent of the stretch can be understood with the definite integral in x_k between 0 and x_0 such that:

$$\int_0^{x_0} \partial x_t = \int_0^{x_0} \partial x_1 + \iint_{0,0}^{x_0, x_k} \partial x_k \partial x_{k+1} + \iiint_{0,0,0}^{x_0, x_k, x_{k+1}} \partial x_k \partial x_{k+1} \partial x_{k+2} + \dots$$

$$x_t = x_0 + \frac{x_0^2}{2!} + \frac{x_0^3}{3!} + \dots$$

Increasing the boundary conditions defines all equal naturally occurring equations while using the boundary condition of 1 as the origin of our system of math used to coincide with the counting of sheep for trade we arrive at the Taylor Series.

Defining complex i as a vector orthogonal to a real stretch or stretch in x using ix in equation M3 we arrive at $P_{ix} = e^{ix} - 1$. This indicates that orthogonal growth forces spin which creates the perception of physical Euclidean space through an oscillating compression and expansion of empty space. The separation of a "2 dimensional spin" creates a dynamic metric space when j is perceived as propagation in "imaginary 2D orthogonal growth i and j ".

Equation M2, better understood as the Two Dimensional Euler equation, predicts this element where $e^{ix} - 1$ and the residual $e^{i\omega t j}$ is perceived as propagation. In our current construct of Quantum Electrodynamics $e^{ix} - 1$ predicts the uncertainty principal as an expansion and compression of physical dynamic space while what we perceive as propagation is predicted by $e^{i\omega t j}$. By using the one dimensional Euler equation to develop the Schrödinger equation, $e^{ix} - 1$ becomes embedded and i spin is accounted for by the uncertainty principal. See C Particle Stability in Dynamic space. In this dynamic space $e^{i\omega t j}$ or $e^{j\omega t}$ becomes the ether that defines the space metric. Euclidean space flows from DSM such that a spin radius of $r = r\hat{r}$ defines physical distance $d = re^{j\hat{r}t}$, velocity as $v = jCe^{j\hat{r}t}$ and $a = -\frac{c^2}{r}e^{j\hat{r}t}$. Euclidean space exists relative to this spin $e^{j\omega t}$ but is perceived as real when time is perceived as real and hence fourth Euclidean dimension jCt emerges. Just as the energy of matter exists relative to the Ether or particle-antiparticle quiescent energy $E_q = \frac{3}{8}m_e C^2$ and a frequency of $f_{RAP} = \frac{5.822580631}{2\pi} \times 10^{20}$ Real space exists relative to $e^{j\omega t}$.

Further a spin in dynamic space forces a quasi infinite compression of physical space that we perceive as matter. (see B particle creation in dynamic space)

The concept of quasi infinite can be understood with a sum or product expansion series for any chord length, S_0 to radians, θ can be realized when we assume i to be orthogonal to real space.

$$\lim_{2^n \rightarrow \infty} 2^n \sqrt{2 - \sqrt{2 + \sqrt{2 + \dots \sqrt{4 - S_0^2}}} = \frac{k\pi}{2}; 0 \leq S_0 \leq \sqrt{2}$$

$$\frac{\pi}{2} = 2$$

$$- \sum_1^{2^n = \infty} 2^n \left(\frac{2 - \sqrt{2 + \sqrt{2 + \dots \sqrt{2}}}}{\sqrt{2 + \sqrt{2 + \dots \sqrt{2}}}} \right) \left(\frac{\sqrt{2 - \sqrt{2 + \sqrt{2 + \dots \sqrt{2}}}}}{2 + \sqrt{2 + \sqrt{2 + \dots \sqrt{2}}}} \right)$$

The author developed numerous sum and product series identities for $k\pi; 0 \leq k \leq 2\pi$ that converged as $x \rightarrow \infty$ and $x = 2^n$ is the number of inscribed sides.

Although beyond the scope of this paper $\frac{\ln \infty}{\ln 2}$ is said not to exist given that it is accepted that $\ln \infty = \infty$ and proven

using limits. Given all of the above identities flow from the accepted definitions of π and converge at $2^n = \infty$ there is a direct correlation between the number of sides as a function of n and the area or length as a function of n . If the assumption that $\ln \infty = \infty$ or $\infty = 2^\infty$ then using $n = 2^n$ in this infinite series should yield the same answer for $\frac{\pi}{2}$ but it obviously does not. A better understanding of infinity relies on its rate of dimensional divergence or rate at which it approaches zero in the next orthogonal dimension.

As $x \rightarrow \infty; \ln x = x \therefore \ln(x-1) = x-1$.

And $\frac{d \ln x}{dx} = \frac{1}{x}$ and $\frac{dx}{dx} = 1$. Clearly for large $x; \frac{d \ln x}{dx} \rightarrow 0$ and $\ln x = \ln(x-1)$ BUT $x \neq x-1$.

The use of limits to prove $\ln \infty = \infty$ fails to account for the rate of approach. If ∞ is to be consistent with the rules of mathematics just as we have shown there are different degrees of zero we must also understand different degrees of ∞ . The intention here is to provide a cursory understanding of these elements and how everything gets created from nothing. However abstract they may be, they lead us back to a more Newtonian understanding of the universe where an attempt to use Quantum analysis leads us to a probability based explanation of this nothingness. Although a simple algebraic manipulation of Viète's formula yields $\lim_{n \rightarrow \infty}$ versus our $\lim_{2^n \rightarrow \infty}$ the difference, however subtle yields great insight.

NOTE: D'Alembert in Minkowski space is consistent with $x^2 + y^2 = (Ct)^2$ or $x^2 + y^2 + (iCt)^2 = 0$, however in this metric space, time and space are parallel and confluent.

Hence $\|s\| = \|Ct\| = \sqrt{x^2 + y^2 + z^2} = Ct$ (M2)

The following metric exists given a relative motion between A and B of u_x, u_y, u_z . If $u_x = 0, u_y = 0$ and $u_z = 0$; the metric stands in a static space. The most important observation here is that an event at A and an event at B are separated by a metric of both space and time and cannot experience an event simultaneously.

$$d(A, B) = \|A - B\|$$

$$= \sqrt{(x_A - x_B + u_x t)^2 + (y_A - y_B + u_y t)^2 + (z_A - z_B + u_z t)^2}$$

$$= \sqrt{(C_{xA}t_A - C_{xB}t_B)^2 + (C_{yA}t_A - C_{yB}t_B)^2 + (C_{zA}t_A - C_{zB}t_B)^2}$$

$d_t(A, B) = \|t_A - t_B\| = \sqrt{\left(\frac{x_A - x_B}{c}\right)^2 + \left(\frac{y_A - y_B}{c}\right)^2 + \left(\frac{z_A - z_B}{c}\right)^2}$ The normalized inner product

$$\mathbf{x} \cdot \mathbf{y} = 0; \mathbf{y} \cdot \mathbf{z} = 0; \mathbf{x} \cdot \mathbf{z} = 0; \mathbf{s} \cdot \mathbf{t} = 1$$

$$\sqrt{s \cdot t} = \sqrt{t \cdot t} = \sqrt{s \cdot s} = \|s\| = \|t\|$$

$$\mathbf{s} \cdot \mathbf{s} = Ct \cdot Ct = \mathbf{s} \cdot \mathbf{s} = s^2 = Ct^2 = \|s\|^2 = \|Ct\|^2$$

$$\mathbf{x} \cdot C_x t = C_x t \cdot C_x t = (C_x t)^2$$

$$\mathbf{y} \cdot C_y t = C_y t \cdot C_y t = (C_y t)^2$$

$$\mathbf{z} \cdot C_z t = C_z t \cdot C_z t = (C_z t)^2$$

$$\mathbf{x} \cdot C_x t + \mathbf{y} \cdot C_y t + \mathbf{z} \cdot C_z t = \mathbf{s} \cdot \mathbf{s} = Ct \cdot Ct = s^2 = Ct^2 = \|s\|^2 = \|Ct\|^2$$

Therefore the dot product of space and time forces Pythagoras and static Euclidean Space.

This allows for simple translations to equate relative times and relative distances. Preservation of physical space in the local frame predicts calculus, momentum and forces.

The inability to perceive relative motion forces relativity and the constancy of C . It is in fact the same

photon defining space in both frames. A photon in the reference frame moving at u_x, u_y and $\theta = \tan^{-1} \frac{u_y}{u_x}$ appears to have no u_x relative to a particle traveling at u_x and hence the u_y motion is the tangential velocity ($\theta = 90^\circ$) of the photon experienced in the moving frame and hence $y' = \frac{\sqrt{C^2 - u_x^2}}{C} y$. The speed of light is constant in every frame (because the same light particle defines space in both frames) however relative velocity of the frame creates a relative velocity of C.

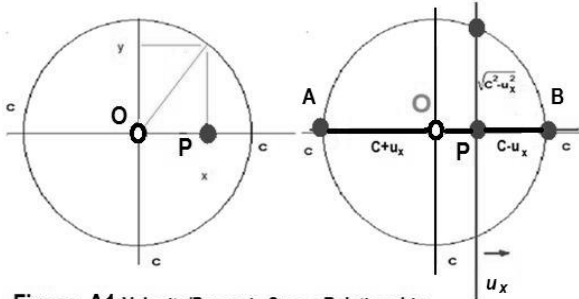


Figure A1 Velocity/Dynamic Space Relationship

In Dynamic space physical space becomes spherical. This spherical dynamic space distorts the distance perceived between a static object O and a Particle P moving at velocity u_x . Distance between the solid dots becomes the new x,y,z Norm (distance) in the moving frame. Distance in the reference frame remains Ct isotropically, while the norm in the direction of travel for example becomes $(C-u_x)t$.

A transform in this dynamic space using a simple Galilean transform where physical space S transforms to S' is derived as the relationship between Norms in relative frames using a universal time. Where $S = Ct$ in the reference frame and velocity in S' is a function of u_x such that $S' = f(u_x)t$, where the direction of velocity dictates the x axis for ease of calculations.

$$S(x, y, z) \xrightarrow{u_x} S'(x', y', z')$$

$$x' = (C - u_x)t$$

$$x = Ct$$

$$\frac{x'}{x} = \frac{(C - u_x)t}{Ct}$$

Distance in direction of u_x : $x' = \frac{(C - u_x)}{C} x$

Distance behind direction of u_x $x' = \frac{(C + u_x)}{C} (x)$

$$y' = \frac{\sqrt{C^2 - u_x^2}}{C} y$$

$$z' = \frac{\sqrt{C^2 - u_x^2}}{C} z$$

This simple Galilean or Newtonian transform in this dynamic space predicts: SRT, the Lorentz transform and the Doppler effect and the Sagnac correction factor for GPS.^{xi xii}

If one is compelled to understand relative rates of clocks given that in the inertial or reference frame $x=y=z=Ct$ a time lag or phase shift can be calculated between frames. (Given that this model predicts the Sagnac correction factor for GPS a likely more efficient method for GPS calculations would be a determination of the time lag created by the norm between the Satellites and the object P)

$$S_t(x, y, z) \xrightarrow{u_x} S'_t(x', y', z')$$

Time lead in direction of u_x $t'_x = \frac{C}{(C - u_x)} t_x$

Time lag behind direction of u_x $t'_x = \frac{C}{(C + u_x)} (t_x)$

$$t'_y = \frac{C}{\sqrt{C^2 - u_x^2}} t_y$$

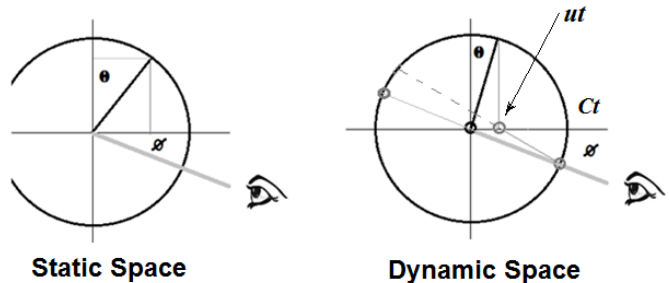
$$t'_z = \frac{C}{\sqrt{C^2 - u_x^2}} t_z$$

If A and B fig. 1A are one light year apart, they both experience a one year phase shift in time relative to the other even if they are in the same static frame. It is a simple exercise to demonstrate that if a clock at P is switched on as it leaves A and switched off when it arrives at B and notification time of one year is permitted for the clock pulses to arrive back at A all will count the same number of clock pulses. This is regardless of velocity and resultant frequency changes (rate of clocks) and the change in phase shift is a function of the distance P travels and not the velocity of P.

The obvious advantage of this space is that Minkowski space and the Lorentz transform become a single element of the entire space metric and spin and rotation in the direction of propagation can be inserted into the space to account for an acceleration of physical space which is perceived as EM and gravity forces respectively. (See D Spin Induced fields of Force and E Rotation Induced Fields of Force.

B Relativistic Doppler Illusion

Observation in dynamic space causes a parallax, which manifests itself as Special Relativity. In Ives Stillwell a mirror was placed to reflect the light emitted so the observer in the static space measured the light emitted forwards and backwards by the particle moving at ut .



The distance to and from the observers direction to the new space origin or grey O at $\frac{ut}{Ct}$ in normalized space:

$$\sqrt{\sin^2 \theta + \left(\cos \theta - \frac{u}{C}\right)^2} \sqrt{\sin^2 \theta + \left(\cos \theta + \frac{u}{C}\right)^2}$$

Expanding and summing the total distance we arrive at:

$$\sqrt{1 + \left(-2\frac{u}{C} \cos \theta + \left(\frac{u}{C}\right)^2\right)} + \sqrt{1 + \left(2\frac{u}{C} \cos \theta + \left(\frac{u}{C}\right)^2\right)}$$

Using a first order approximation we get;

$$1 - \frac{u}{C} \cos \theta + \frac{1}{2} \left(\frac{u}{C}\right)^2 + 1 + \frac{u}{C} \cos \theta + \frac{1}{2} \left(\frac{u}{C}\right)^2 = 2 + \left(\frac{u}{C}\right)^2$$

For the special case where the observer is in the direct propagation path no parallax is observed. Both of these results are confirmed by GPS where the $\frac{1}{2} \left(\frac{u}{C}\right)^2$ stretch is accounted for between land based clocks and satellite clocks while simple Doppler observed above is used to synchronize

Satellite based clocks and this is referred to as the Sagnac correction factor.^{xi,xii}

C Particle Creation in Dynamic space

In circular motion $\theta = \frac{u_x t}{R}$ is the distance traveled in radians. If we let d_t equal the distance tangential to the direction of motion it follows that $(d_t)^2 + (u_x t)^2 = (Ct)^2$ becomes $(d_t)^2 + \left(2R \sin \frac{\theta}{2}\right)^2 = (Ct)^2$

$$(d_t)^2 = (Ct)^2 - \frac{\left(2R \sin \frac{u_x t}{2R}\right)^2}{(Ct)^2} (Ct)^2$$

$$\frac{Ct}{d_t} = \left(1 - \left(\frac{2R \sin \frac{u_x t}{2R}}{Ct}\right)^2\right)^{-\frac{1}{2}}$$

If we let the velocity $u_x = C$ we arrive at a *sincx* function

$$\frac{Ct}{d_t} = \left(1 - \left(\frac{\sin \frac{Ct}{2R}}{\frac{Ct}{2R}}\right)^2\right)^{-\frac{1}{2}}$$

Hence if a point begins to spin at C at $t=0 + \frac{\sin \frac{Ct}{2R}}{\frac{Ct}{2R}} \rightarrow 1$ a

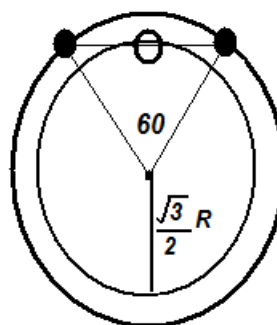
quasi- infinite compression of tangential physical space is experienced, where $d_t = 0 \times Ct$ at $\theta=0+$ while at $\theta = \pi$ compression is reduced to $d_t \sim 1.3 Ct$ and no compression exists at $\theta = 2\pi$.

As this circular motion continues the periodic contraction diminishes to zero as rotation occurs at $x = \pi$ or $\theta = 2\pi$.

Therefore if a point C begins to spin at the speed of light, physical space in this dynamic space contracts quasi infinitely in the tangential direction BC or \overline{BC} .

D Particle Stability in Dynamic space

Particle stability in this dynamic space is assumed to occur when two points A and B satisfy the condition of $d = Ct$ or $\overline{AB} = Ct$ where distance d or \overline{AB} is a fixed distance. The condition for these two points to be stable exists when both points spin in the same direction at the speed of light and out of phase by 60 degrees from $|Ce^{j\theta} - Ce^{j(\theta+60)}| = C$.



Particle Pair

$$\text{Radius} = \frac{\sqrt{3}}{2} R$$

$$\text{Velocity} = \frac{\sqrt{3}}{2} C$$

Fig. A3 Stable Particle in Dynamic Space

E Spin Induced Field Creation in Dynamic space

An acceleration of free space is created by particle spin and is referred to as a Spin Induced Field. Although related to Spin in Physics they are not synonymous. It is a simple exercise to demonstrate that Spin creates a repulsive acceleration of free space while rotation in the direction of propagation creates an attractive acceleration of free space. These are perceived as forces.

In Figure A4 we define a point in space as a point particle S_p and note that an angle θ is created where S_p experiences the maximum and minimum velocity of the particle spin such that $\theta = \cos^{-1} \frac{R_p}{r}$. A first order model of these fields can be made by making a few model simplifications. The perceived force of the photon is calculated by averaging the acceleration and deceleration of the particle through half a cycle. Since $\theta < \frac{\pi}{2}$ the net acceleration separates the particle and S_p . Although symmetry exists about the x axis in static space, this dynamic space is warped since in far field S_p experiences the particle spin from 0 to π receding and π to 2π approaching and this lack of relative dynamic symmetry creates the perpendicular force field.

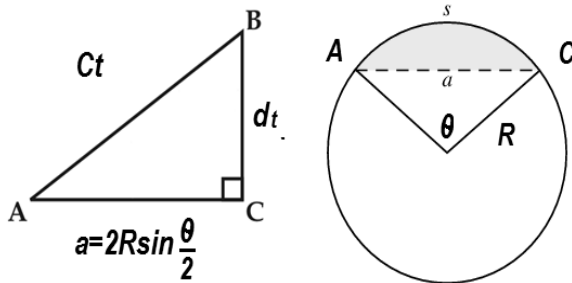


Fig. A2 Circular Motion at C and Tangential Space

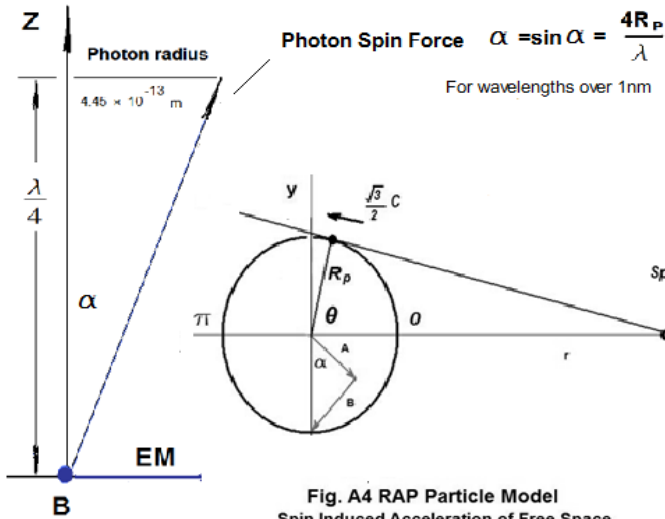


Fig. A4 RAP Particle Model
Spin Induced Acceleration of Free Space

$$\frac{F_{acc}}{S_p} = \frac{\Delta v}{\Delta t} = \frac{3}{4} \frac{C^2}{R_p \theta} ; \quad \frac{F_{dec}}{S_p} = -\frac{3}{4} \frac{C^2}{R_p (\pi - \theta)}$$

$$\frac{F_{net}}{S_p} = \frac{3}{4} \left(\frac{C^2}{R_p \theta} + \frac{-C^2}{R_p (\pi - \theta)} \right)$$

For large distances (far field) $r \gg \theta = \frac{\pi}{2} - \frac{R_p}{r}$ and $\frac{F_{net}}{S_p} = \frac{6C^2}{\pi^2 r}$.

It should be noted that the approximations fail as r approaches R_{RAP} .

Analysis of S_p from $\theta = 0 \rightarrow \pi$ yields vector A as the average deceleration force and B is the average acceleration force then: $|A + B| = \frac{v^2}{R} = \frac{3C^2}{4R_p}$ if $r=0$.

Assuming that A and B have an approximate angle $\alpha = 45^\circ$ and the net acceleration is in this direction the x component of a first order model of A+B will then be:

$$\left[\left(\frac{3C^2}{\sqrt{2}4R} + \frac{3C^2}{\pi^2 r} \right) - \left(\frac{3C^2}{\sqrt{2}4R} - \frac{3C^2}{\pi^2 r} \right) \right] \cos 45^\circ = \frac{6C^2}{\sqrt{2}\pi^2 r}$$

The new angle from the y axis of A+B will be:

$$\tan \theta_n \approx \sin \theta_n = \frac{\sqrt{2} 4R_p}{3C^2} = \frac{\sqrt{2} 4R_p}{\pi^2 r}$$

$$\therefore a_x = \frac{6C^2}{\pi^2 r} \left(\frac{\sqrt{2} 4R_p}{\pi^2 r} \right) = \frac{24\sqrt{2}R_p C^2}{\pi^4 r^2} \quad \therefore a_y = \frac{6C^2}{\sqrt{2}\pi^2 r}$$

Both are consistent with the magnetic and electric field associated with the photon. Analyzing this spin in dynamic space we arrive at the dynamic spin factor:

$$\frac{F}{S_p} = \frac{d(\gamma u)}{dt} = \frac{F}{S_p} = \frac{d(\gamma)}{dt} u + \frac{d(u)}{dt} \gamma; \text{ assume } \frac{d(u)}{dt} = 0$$

$$\gamma = \frac{1}{1 + \frac{u}{c}} \quad (0 \rightarrow \pi): \quad \gamma = \frac{1}{1 - \frac{u}{c}} \quad (\pi \rightarrow 2\pi) \quad \bar{v}_{0 \rightarrow \pi} = \frac{\sqrt{3}C}{\pi}$$

Although in static Euclidean Space a_y is symmetrical but opposite from π to 2π in DSM it yields a net perpendicular force $2.738763636 - 0.229088343 = 2.509675293$

$$\frac{F_{net}}{S_p} = \frac{6C^2}{\sqrt{2}\pi^2 r} [2.509675293]$$

Calculating the repulsive force exerted on an electron we arrive at:

$$F_p = \frac{24\sqrt{2}R_p C^2}{\pi^4 r^2} m_e = \frac{127.2886 \times 10^{-28}}{r^2} N \cdot m^2$$

Multiplying this static value by the first order model dynamic spin factor for the photon of 2.509675293 we arrive at a force about 138.5 times greater than an electron would exert on another electron at the same distance. It is this force that prevents particulates from collapsing on each other and must be overcome to bind the particulate to make three-dimensional particles. This spin induced force is likely the real component of the apparent Strong Force as centripetal is the real element of the apparent centrifugal force. It is this force that was used to develop the photon particle model.

A similar model for the electron can be approximated using the Bohr radii and $\frac{R_p}{R_{RAP}}$ to compensate for the cosine effect of the force which predicts a force about 100.09% of that predicted by Coulomb's law well within the error for first order model assumptions.

$$F_p = \frac{R_p}{R_{RAP}} \frac{24\sqrt{2}R_p C^2}{\left(\frac{a_0}{R_p} + \frac{2}{\sqrt{3}} \right) \pi^4 (r)^2} m_e (2.5096)$$

$$= \frac{2.3065 \times 10^{-28}}{r^2} N \cdot m^2$$

F. Rotation Induced Field Creation in Dynamic space

A first order model to derive the gravitational constant for the electron relative to the Ether using $1.5 a_0$ as the radius of rotation or propagation radius yields:

$$G = \frac{6C^2}{\pi^2 r} \frac{R_p}{r} \frac{R_p}{1.5a_0} R_{RAP} = 6.78989879 \times 10^{-11} \frac{m^3}{kg \cdot s^2}$$

where a_0 is the Bohr radius

This yields an error 1.7% above current theory given the model assumptions .

ⁱ Paul A. Tipler, Physics, Worth Publishers, 1979 pg 579

ⁱⁱ Haskell, Richard "A Simple Experiment on Fresnel Diffraction" AJP, 1969

ⁱⁱⁱ Horiba Scientific, A Guide Book to Particle Size Analysis

^{iv} Browne, M.W. "Lockheed credits Soviet theory in design of F-117",

Aviation Week Space Technology p. 27, December 1991

^v Photonics Research Project: Unified Theory, 2013 Jake

Bonsignore, Jon Brule, Photonics Department, Niagara College

^{vi} Microwave Engineering, Second Edition, David A. Pozar

^{vii} Experimental Observation of a Photon Bouncing Ball, G. Della Valle et al, PRL 102, 180402 (2009)

^{viii} Stephen Boughn. **Fritz Hasenöhrl and $E = mc^2$** . *The European Physical Journal H*, 2013

^{ix} Zeeya, Morali (26 August 2006). "[Ether returns to oust dark matter](#)". *New Scientist*. Retrieved 27 August 2012.

^x Kragh, Helge (2005). *Dirac. A Scientific Biography*. Cambridge: Cambridge University Press. pp. 200–203

^{xi} CCIR *Internat. Telecom, Union Annex to Vol 7*, No: 439-5. Geneva 150-4 (1990)

^{xii} A. G. Kelly, "*The Sagnac Effect and the GPS Synchronization of Clock-Stations*" Ph. D. HDS Energy Ltd., Celbridge, Co. Kildare, Ireland. Also, A. G. Kelly, Inst. Engrs. Ireland 1995 and 1996, Monographs 1 & 2.